# The Reaction of Acetylene with Hydroxyl Radicals

**Juan P. Senosiain, Stephen J. Klippenstein, and James A. Miller***

*Combustion Research Facility, Sandia National Laboratories, Livermore, California 94551-0969*

*Received: February 10, 2005; In Final Form: May 3, 2005*

The potential energy surface for the reaction between OH and acetylene has been calculated using the RQCISD(T) method and extrapolated to the complete basis-set limit. Rate coefficients were determined for a wide range of temperatures and pressures, based on this surface and the solution of the one-dimensional and two-dimensional master equations. With a small adjustment to the association energy barrier (1.1 kcal/mol), agreement with experiments is good, considering the discrepancies in such data. The rate coefficient for direct hydrogen abstraction is significantly smaller than that commonly used in combustion models. Also in contrast to previous models, ketene + H is found to be the main product at normal combustion conditions. At low temperatures and high pressures, stabilization of the $C_2H_2OH$ adduct is the dominant process. Rate coefficient expressions for use in modeling are provided.

## I. Introduction

The reaction of acetylene with hydroxyl radicals is important in combustion,[1] atmospheric,[2] and astrophysical[3] processes. Acetylene is one of the major intermediates of rich hydrocarbon flames, and its reaction with OH can be an important degradation pathway.[4,5] The rate and mechanism of this reaction have a strong influence on the post-flame behavior of small hydrocarbons, and the resulting radicals are potentially crucial in the NO chemistry[1,6] of the flame. Because of its significance, this reaction has been the subject of numerous experimental studies.[6−39] However, to our knowledge, there has been only one comprehensive theoretical investigation of the kinetics of the title reaction.[40]

At low temperatures, the reaction between OH and $C_2H_2$ proceeds by simple electrophilic addition. The resulting intermediate can be stabilized by collisions with a third body or dissociate back to reactants, resulting in a pressure dependence and markedly non-Arrhenius behavior:

$$OH + C_2H_2 \rightarrow HOC_2H_2^*$$
$$HOC_2H_2^* \rightarrow OH + C_2H_2$$
$$HOC_2H_2^* + M \rightarrow HOC_2H_2 + M$$

The pressure dependence has been studied extensively at room temperature;[16,18,19,22,23,33,34,39] but, data at other temperatures are limited.[16]

At higher temperatures, direct hydrogen abstraction, as well as isomerization of the addition complex and subsequent dissociations, giving rise to several bimolecular channels:

$$OH + C_2H_2 \rightarrow H_2O + C_2H \quad (1)$$
$$\rightarrow H + HCCOH \quad (2)$$
$$\rightarrow H_2 + HCCO \quad (3)$$
$$\rightarrow H + CH_2CO \quad (4)$$
$$\rightarrow CH_3 + CO \quad (5)$$

In most of the high-temperature studies, rate coefficients were obtained indirectly. The difficulty of deconvoluting flame or shock-tube data has resulted in a lack of consensus for the rate coeffcients and product branching ratios at high temperatures. For example, the shock-tube experiments by Hwang and coworkers[25] found rate coefficients for channels other than hydrogen abstraction that are markedly higher than those of ref 40. Later, atmospheric flame studies by Kaiser[29] and Woods and Haynes[6] coincided roughly with ref 40 and older values of this rate coefficient.[7,17] Nonetheless, newer counter-flow flame studies by Waly et al.[36,37] required the value of $k_4$ to be substantially higher to reconcile their numerical model with measured profiles.

There have been several first-principles studies of the $C_2H_3O$ potential energy surface (PES). With the exception of the papers by Miller and Melius,[40] Ding et al.[41] and Carl et al.,[42] these have concentrated on single elementary steps.[34,38,43−52] Other theoretical works have studied the kinetics of the related H + $CH_2CO$[38] and $H_2O$ + $C_2H$[41] reactions, as well as the decomposition of acetyl[46,53−55] and vinoxy radicals.[43,48,54,57,58]

Currently, many combustion models use rate coefficients that have been derived from the theoretical work of Miller and Melius.[40] Since this study, progress in the fields of theoretical chemical kinetics and quantum chemistry has been such that a theoretical re-examination of this reaction is warranted. The present work uses a high-level potential energy surface and state-of-the-art, master-equation methods to compute the rate coefficients as a function of temperature and pressure and to clarify existing questions about the product branching ratios.

## II. Quantum Chemistry and the $C_2H_3O$ Potential Energy Surface

In order to calculate accurate rate coefficients, energies, frequencies, and torsional potentials need to be evaluated at several geometries along the intrinsic reaction coordinate (IRC). These were computed using density functional theory (DFT) with the hybrid B3LYP functional[59,60] in its spin-unrestricted form and the 6-311++G(d,p) basis set. This method has been shown to achieve accurate geometries, zero-point energies (ZPEs),[61] and frequencies[62] while having a high computational efficiency. Vibrational frequencies and rotational constants of

* Corresponding author. Address: P.O. Box 969, M. S. 9055, Livermore, CA 94551-0969, USA. Phone: +1 925 294-2759. Fax:+1 925 294-2276. E-mail: jamille@sandia.gov.

10.1021/jp050737g CCC: $30.25 
Published on Web 06/17/2005

**TABLE 1: Rovibrational Properties of Reactants, Intermediates, and Bimolecular Products**

| | species | rotational constants ($cm^{-1}$) | $\sigma_{rot}$[a] | $m$[b] | frequencies ($cm^{-1}$)[c] |
|---|---|---|---|---|---|
| **R** | $C_2H_2$ | 1.187, 1.187 | 2 | 1 | 649, 649, 775, 775, 2062, 3417, 3520 |
| | OH | 18.672, 18.672 | 1 | 1 | 3710 |
| **C1** | $OH\cdots C_2H_2$ | 1.185, 0.150, 0.133 | 2 | 1 | 71, 110, 213, 390, 662, 687, 778, 792, 2057, 3411, 3514, 3631 |
| **C2** | $OH\cdots C_2H_2$ | 1.281, 0.242, 0.206 | 1 | 2 | 72, 129, 203, 469, 656, 668, 773, 779, 2027, 3419, 3518, 3745 |
| **1a**[d] | HOCHCH | 2.623, 0.363, 0.319 | 1 | 1 | **459**, 471, 568, 760, 838, 1095, 1237, 1352, 1663, 3106, 3303, 3793 |
| **1b** | | 2.168, 0.378, 0.322 | 1 | 1 | **434**, 439, 578, 752, 902, 1045, 1233, 1357, 1649, 3166, 3291, 3807 |
| **1c** | | 2.887, 0.355, 0.316 | 1 | 1 | **238**, 483, 589, 753, 810, 1100, 1257, 1316, 1699, 3051, 3302, 3859 |
| **1d** | | 2.326, 0.372, 0.321 | 1 | 1 | **212**, 437, 604, 783, 869, 1058, 1236, 1329, 1682, 3117, 3298, 3841 |
| **2** | $OCHCH_2$ (A″) | 2.247, 0.382, 0.326 | 2 | 1 | **443**, 507, 760, 975, 978, 1157, 1395, 1471, 1545, 2943, 3138, 3253 |
| **2** | $OCHCH_2$ (A′) | 2.524, 0.365, 0.319 | 2 | 1 | **431**, 710, 815, 950, 970, 1083, 1240, 1435, 1593, 2990, 3169, 3271 |
| **3** | $HOCCH_2$ | 3.570, 0.335, 0.310 | 1 | 2 | **351**, 445, 625, 826, 960, 1121, 1220, 1404, 1707, 3092, 3221, 3802 |
| **4** | $OCCH_3$ | 2.822, 0.333, 0.315 | 3 | 1 | **121**, 473, 852, 950, 1054, 1356, 1451, 1458 ,1925, 3022, 3109, 3113 |
| **5** | $H(COC)H_2$ | 1.000, 0.789, 0.497 | 1 | 2 | 770, 796, 937, 1038, 1068, 1124, 1177, 1352, 1520, 3093, 3132, 3186 |
| **P1** | $C_2H$ | 1.483, 1.483 | 1 | 1 | 303, 303, 2083, 3458 |
| | $H_2O$ | 27.523, 14.339, 9.427 | 2 | 1 | 1602, 3818, 3924 |
| **P2** | H + HCCOH | 22.645, 0.326, 0.321 | 1 | 1 | 396, 444, 554, 651, 1085, 1243, 2278, 3492, 3785 |
| **P3** | HCCO | 43.005, 0.364, 0.361 | 1 | 1 | 428, 502, 556, 1268, 2088, 3354 |
| | $H_2$ | 60.411, 60.411 | 2 | 1 | 4418 |
| **P4** | $H + CH_2CO$ | 9.498, 0.344, 0.332 | 2 | 1 | 445, 555, 602, 988, 1170, 1406, 2221, 3176, 3269 |
| **P5** | $CH_3$ | 9.548, 9.548, 4.774 | 3 | 1 | 537, 1403, 1403, 3103, 3283, 3283 |
| | CO | 1.933, 1.933 | 1 | 1 | 2212 |

[a] Symmetry numbers, including internal rotors. [b] Number of optical isomers, adjusted in cases with internal rotors. [c] Torsional modes treated as internal rotors are shown in bold type. [d] Conformers **1a**−**1d** have been treated as a single species (see text for details).

**TABLE 2: Rovibrational Properties of First-Order Saddlepoints**

| transition state | rotational constants ($cm^{-1}$) | $\sigma_{rot}$[a] | m[b] | frequencies ($cm^{-1}$)[c] |
|---|---|---|---|---|
| **1a ↔ 1b**[d] | 2.421, 0.366, 0.318 | 1 | 1 | 558 i, 469, 491, 522, 873, 1033, 1220, 1359, 1660, 3113, 3436, 3793 |
| **1a ↔ 1c** | 2.626, 0.353, 0.320 | 1 | 1 | 411 i, 461, 666, 768, 803, 1072, 1207, 1293, 1658, 3040, 3277, 3822 |
| **1b ↔ 1d** | 2.051, 0.376, 0.327 | 1 | 1 | 379 i, 423, 680, 817, 874, 1013, 1196, 1306, 1639, 3126, 3274, 3819 |
| **1c ↔ 1d** | 2.682, 0.358, 0.316 | 1 | 1 | 567 i, 244, 515, 530, 838, 1038, 1237, 1332, 1696, 3045, 3447, 3833 |
| **1 ↔ 2** | 1.791, 0.458, 0.366 | 1 | 2 | 2017 i, 312, 808, 902, 1005, 1094, 1159, 1304, 1399, 1995, 3124, 3170 |
| **1 ↔ 3** | 3.482, 0.334, 0.311 | 1 | 2 | 1867 i, 330, **476**, 546, 606, 819, 1001, 1236, 1786, 2284, 3152, 3806 |
| **2 ↔ 3** | 3.968, 0.327, 0.302 | 1 | 2 | 2045 i, 357, 433, 553, 764 , 955, 1122, 1400, 1681, 2408, 3115, 3241 |
| **2 ↔ 4** | 3.391, 0.341, 0.321 | 1 | 2 | 1543 i, 437, 633, 852, 1032, 1122, 1211, 1448, 1830, 1901, 3041, 3232 |
| **2 ↔ 5** | 1.173, 0.604, 0.433 | 1 | 2 | 1128 i, 564, 833, 882, 1037, 1090, 1307, 1348, 1489, 3094, 3161, 3195 |
| **3 ↔ 4** | 2.475, 0.389, 0.352 | 1 | 2 | 2383 i, 288, 596, 772, 969, 991, 1103, 1397, 1441, 1756, 3095, 3203 |
| **1 → P2** | 3.250, 0.326, 0.296 | 1 | 1 | 468 i, **243**, 420, 448, 477, 544, 656, 1079, 1246, 2211, 3484, 3742 |
| **2 → P4** | 2.933, 0.336, 0.311 | 1 | 2 | 789 i, 315, 486, 522, 593, 635, 995, 1143, 1405, 2140, 3163, 3279 |
| **3 → P1** | 2.140, 0.364, 0.319 | 1 | 2 | 1832 i, 410, 490, 626, 709, 817, 976, 1173, 1651, 1726, 3307, 3745 |
| **3 → P2** | 3.359, 0.303, 0.285 | 1 | 1 | 378 i, **102**, 230, 399, 476, 650, 660, 1091, 1239, 2240, 3474, 3774 |
| **3 → P4** | 4.829, 0.317, 0.297 | 2 | 1 | 1441 i, **249**, 355, 538, 669, 708, 981, 1141, 1403, 2045, 3122, 3225 |
| **4 → P4** | 2.988, 0.310, 0.298 | 1 | 1 | 330 i, 253, 413, 462, 559, 705, 998, 1150, 1398, 2212, 3173, 3267 |
| **4 → P5** | 1.950, 0.226, 0.211 | 1 | 3 | 275 i, **15,** 240, 459, 503, 815, 1407, 1414, 2091, 3094, 3259, 3272 |
| **R ↔ 1** | 1.435, 0.268, 0.227 | 1 | 1 | 209 i, **72**, 228, 630, 646, 666, 769, 802, 1975, 3414, 3504, 3757 |
| **R ↔ P1** | 6.591, 0.165, 0.163 | 1 | 1 | 669 i, 91, **143**, 343, 571, 607, 684, 1384, 1886, 2086, 3433, 3794 |

[a] Symmetry numbers, including internal rotors. [b] Number of optical isomers, adjusted in cases with internal rotors. [c] Torsional modes treated as internal rotors shown in bold type. [d] Conformers **1a**−**1d** are treated as a single species (see text for details).

the stable intermediates and transition states involved are provided in Tables 1 and 2, respectively.

Unfortunately, the energies obtained with this model chemistry are insufficiently accurate for the purpose of calculating chemical kinetics. For this use, we carried out calculations with the restricted quadratic configuration−interaction method, with single and double excitations and a perturbative treatment of triple excitations,[63] using Dunning's correlation-consistent triple-$\zeta$ and quadruple-$\zeta$ basis sets, i.e., RQCISD(T)/cc-pV$n$Z, $n = \{3,4\}$. Here, the RQCISD(T) method was preferred over the similar RCCSD(T) method, because our own unpublished tests showed that the RCCSD(T) yielded an unphysical turnover in simple bond dissociation potentials at shorter separations than does RQCISD(T). DFT calculations were made using Gaussian 98;[64] all other quantum chemistry calculations were performed using the MolPro collection of programs.[65]

Following the work of Martin[66] and Feller and Dixon,[67] the final energies were then computed by extrapolating to the complete-basis-set (CBS) limit, using the following expression:

$$E_\infty = E_{l_{max}} - \frac{B}{(l_{max}+1)^4} \qquad (6)$$

where $l_{max}$ is the maximum component of angular momentum in the basis set and $E_\infty$ is the CBS energy.[68] The related RCCSD(T) method has been shown to achieve "chemical accuracy", even in situations where spin contamination would normally be a problem (see, for example, ref 69).

The energies of the stationary points on the potential energy surface are provided in Tables 3 and 4 and are illustrated in Figure 1. We note that our attempts to optimize the saddlepoint corresponding to the **3 → P3** transition state using the UB3LYP method were unsuccessful, yielding a structure corresponding to the transition state for the $H + CH_2CO \rightarrow H_2 + HCCO$ reaction. Thus, the geometry of the **3 → P3** transition state was optimized using the UMP2 method.[70] The energies calculated

**TABLE 3: Calculated Energies, Q1 Diagnostic and Zero-Point Energy of Reactants, van der Waals Complexes, Intermediates, and Bimolecular Products**

| | | | calculated energy (kcal/mol) | | | | | |
|---|---|---|---|---|---|---|---|---|
| | symmetry | species | $E_0$[a] | $E_0$[b] | $E_0$[c] | $E_0$[d] | Q1 diagnostic[b,e] | zero-point energy, (kcal/mol)[a] |
| **R** | $^1\Delta$ | $C_2H_2$ | 0.0 | 0.0 | 0.0 | 0.0 | 0.014 | 22.2 |
| | $^2\Pi$ | OH | | | | | 0.007 | |
| **C1** | $^2B_1$ | $OH\cdots C_2H_2$ | −1.6 | −2.0 | −2.0 | | 0.011 | 23.3 |
| **C2** | $^2A$ | $OH\cdots C_2H_2$ | −1.6 | 0.6 | 0.4 | | 0.017 | 23.5 |
| **1a** | $^2A'$ | HOCHCH | −31.0 | −30.8 | −31.1 | −27.5 | 0.016 | 26.7 |
| **1b** | $^2A'$ | HOCHCH | −29.6 | −29.4 | −29.7 | −26.1 | 0.016 | 26.7 |
| **1c** | $^2A'$ | HOCHCH | −27.3 | −27.2 | −27.6 | −25.3 | 0.016 | 25.9 |
| **1d** | $^2A'$ | HOCHCH | −28.0 | −27.9 | −28.2 | −24.8 | 0.015 | 26.4 |
| **2** | $^2A'$ | $OCHCH_2$ | −38.8 | −35.4 | −35.1 | −32.9 | 0.022 | 26.7 |
| **2** | $^2A''$ | $OCHCH_2$ | −60.8 | −58.3 | −58.3 | −55.5 | 0.023 | 26.5 |
| **3** | $^2A$ | $HOCCH_2$ | −35.6 | −34.5 | −34.8 | −31.4 | 0.019 | 26.8 |
| **4** | $^2A'$ | $OCCH_3$ | −66.0 | −65.0 | −65.1 | −62.9 | 0.022 | 27.0 |
| **5** | $^2A$ | $H(COC)H_2$ | −21.6 | −22.5 | −22.6 | −17.3 | 0.022 | 27.4 |
| **P1** | $^1A_1$ | $H_2O$ | 18.5 | 14.2 | 13.4 | 14.6 | 0.008 | 22.1 |
| | $^2\Sigma^+$ | $C_2H$ | | | | | 0.017 | |
| **P2** | $^1A'$ | HCCOH | 12.9 | 10.7 | 10.5 | 14.0 | 0.013 | 19.9 |
| | $^2S_{1/2}$ | H | | | | | 0.001 | |
| **P3** | $^1A_1$ | HCCO | −26.0 | −21.8 | −21.6 | −16.3 | 0.026 | 18.0 |
| | $^2\Sigma_g$ | $H_2$ | | | | | 0.006 | |
| **P4** | $^1A_1$ | $CH_2CO$ | −24.3 | −23.4 | −23.3 | −20.4 | 0.017 | 19.8 |
| | $^2S_{1/2}$ | H | | | | | 0.001 | |
| **P5** | $^2\Sigma^+$ | CO | −53.9 | −56.9 | −56.1 | −64.2 | 0.019 | 21.8 |
| | $^2A_1$ | $CH_3$ | | | | | 0.006 | |
| | $^1A$ | H(COC)H | 53.8 | 52.2 | 52.3 | | 0.048 | 18.6 |
| | $^2S_{1/2}$ | H | | | | | 0.000 | |
| | $^1A$ | $H_2(COC)$ | 42.4 | 37.8 | 38.4 | 41.4 | 0.020 | 20.1 |
| | $^2S_{1/2}$ | H | | | | | 0.000 | |
| | $^2A'$ | $CHCH_2$ | 63.4 | 65.5 | 67.4 | 61.7 | 0.017 | 22.8 |
| | $^3P_2$ | O | | | | | 0.004 | |
| | $^2A'$ | HCO | 35.3 | 37.8 | 38.8 | 35.6 | 0.026 | 18.9 |
| | $^3B_1$ | $CH_2$ | | | | | 0.012 | |

[a] UB3LYP/6-311++G(d,p) [b] RQCISD(T)/cc-pVQZ. Geometries and ZPE at UB3LYP/6-311++G(d,p). [c] RQCISD(T)/CBS (see text for details). Geometries and ZPE at UB3LYP/6-311++G(d,p). [d] UCCSD(T)/6-311+G(2d,2p)//UB3LYP/6-311G(d,p), from ref 41. [e] See refs 73 and 74.

**TABLE 4: Calculated Energies, Energy Maximum along the Intrinsic Reaction Coordinate ($IRC_{max}$), Q1 Diagnostic and Zero-Point Energy of First-Order Saddlepoints**

| | | calculated energy (kcal/mol) | | | | | | |
|---|---|---|---|---|---|---|---|---|
| transition state | symmetry | $E_0$[a] | $E_0$[b,c] | $E_0$[c,d] | $IRC_{max}$[c,d] | $E_0$[e] | Q1 diagnostic[b,f] | zero-point energy, (kcal/mol)[a] |
| **1a ↔ 1b** | $^2A'$ | −28.8 | −27.7 | −28.1 | | | 0.016 | 25.7 |
| **1a ↔ 1c** | $^2A$ | −25.9 | −26.2 | −26.6 | | −23.3 | 0.015 | 25.8 |
| **1b ↔ 1d** | $^2A$ | −25.6 | −25.8 | −26.2 | | −23.1 | 0.015 | 26.0 |
| **1c ↔ 1d** | $^2A'$ | −26.5 | −25.6 | −26.1 | | | 0.015 | 25.4 |
| **1 ↔ 2** | $^2A$ | 1.5 | 3.8 | 3.9 | | 8.1 | 0.030 | 23.3 |
| **1 ↔ 3** | $^2A$ | 13.6 | 17.2 | 18.2 | | 19.4 | 0.017 | 22.9 |
| **2 ↔ 3** | $^2A$ | −3.3 | −1.1 | −1.2 | | 2.6 | 0.017 | 22.9 |
| **2 ↔ 4** | $^2A$ | −21.9 | −17.9 | −18.3 | | −13.5 | 0.026 | 23.9 |
| **2 ↔ 5** | $^2A$ | −9.5 | −8.1 | −8.4 | | −2.5 | 0.041 | 25.7 |
| **3 ↔ 4** | $^2A$ | 14.2 | 15.2 | 15.2 | | 19.8 | 0.026 | 22.3 |
| **1 ↔ P2** | $^2A'$ | 14.4 | 13.9 | 13.4 | 14.3 | 18.0 | 0.015 | 20.8 |
| **2 ↔ P4** | $^2A$ | −19.1 | −16.1 | −16.2 | −15.3 | −12.8 | 0.022 | 21.0 |
| **3 ↔ P1** | $^2A$ | 38.7 | 38.3 | 38.2 | | 42.0 | 0.036 | 22.3 |
| **3 ↔ P2** | $^2A$ | 13.9 | 13.6 | 13.2 | 14.2 | 17.3 | 0.015 | 20.5 |
| **3 ↔ P4** | $^2A$ | −11.4 | −4.6 | −4.8 | −4.0 | −0.5 | 0.031 | 20.6 |
| **4 ↔ P4** | $^2A'$ | −23.3 | −20.0 | −20.1 | −18.8 | −16.6 | 0.020 | 20.9 |
| **4 ↔ P5** | $^2A'$ | −49.2 | −49.9 | −49.4 | −48.6 | −50.0 | 0.019 | 23.7 |
| **R ↔ 1** | $^2A$ | −1.4 | 2.3 | 1.9 | 2.4 | 2.7 | 0.024 | 23.5 |
| **R ↔ P1** | $^2A$ | 15.9 | 18.1 | 18.0 | 19.0 | 20.1 | 0.028 | 21.5 |

[a] UB3LYP/6-311++G(d,p) [b] RQCISD(T)/cc-pVQZ. [c] Geometries and ZPE at UB3LYP/6-311++G(d,p). [d] RQCISD(T)/CBS (see text for details). [e] UCCSD(T)/6-311+G(2d,2p)//UB3LYP/6-311G(d,p), from ref 41. [f] See refs 73 and 74.

by Ding et al.[41] (also shown in Tables 3 and 4) with the related UCCSD(T) method are considerably different from the RQCISD(T)/CBS energies. These discrepancies are probably due to the insufficiency of the 6-311+G(2d,2p) basis set. On the other hand, the differences between energies obtained with the cc-pVQZ basis set and those extrapolated to the CBS limit using eq 6 are small (in most cases, <0.5 kcal/mol).

Two entrance-channel, van der Waals complexes were found on the UB3LYP surface (**C1** and **C2** in Table 3). The most stable of these (**C1**) has a T-shaped $OH-C_2H_2$ structure with $C_{2v}$ symmetry and is bound by 2.0 kcal/mol (with ZPE). Its structure was predicted in 1987 by the calculations of Sosa and Schlegel;[45] but, it was experimentally observed only recently.[52] The **C2** structure is asymmetric, with a C−O distance of 2.4

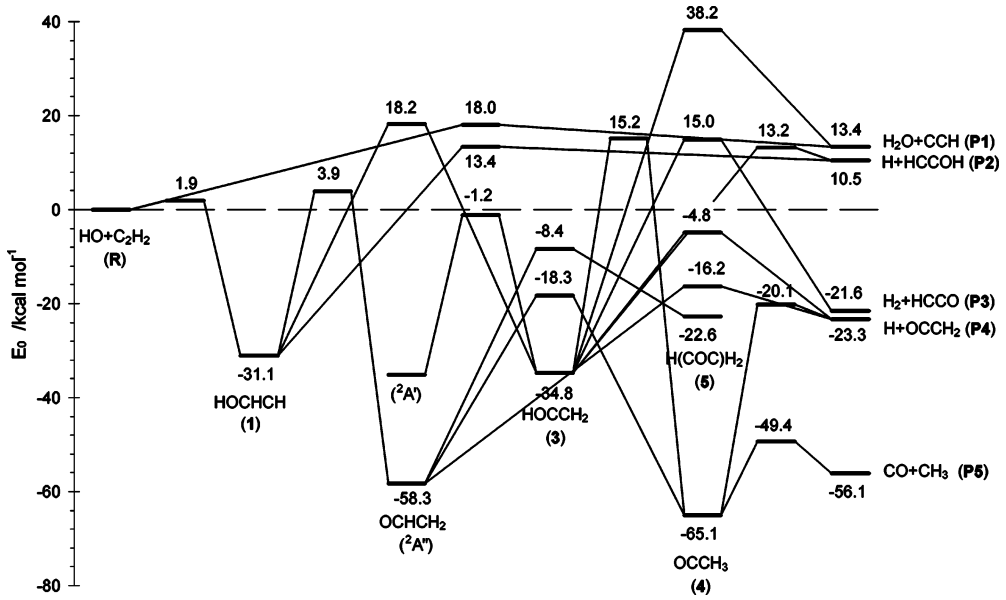


**Figure 1.** Potential energy surface calculated using RQCISD(T)/CBS for electronic energies and UB3LYP/6-311++G(d,p) geometries and zero-point energies. Transition state for **3** → **P3** optimized using UMP2 (see text for details).

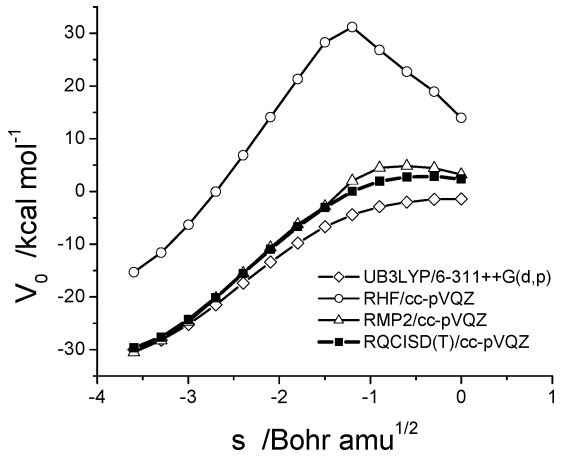


**Figure 2.** Potential energy calculated with several methods on the UB3LYP/6-311++G(d,p) IRC corresponding to the association of OH and $C_2H_2$. Energies include density functional theory (DFT) zero-point energy (ZPE) corrections.

Å; it is bound by 0.9 kcal/mol. There has been some discussion of the importance of van der Waals complexes like these in the kinetics of bimolecular reactions.[71−75] However, in this case, the energy of the transition state for the association of OH and $C_2H_2$ is above the entrance channel, so such complexes are unlikely to play an important role in the kinetics at all but very low temperatures.

Figure 2 shows the energies calculated with different methods along the UB3LYP/6-311++G(d,p) intrinsic reaction coordinate (IRC) for the association of OH with acetylene. The sharp peak in the RHF curve observed at $s = -1.1982$ amu$^{1/2}$ Bohr indicates that the transition state lies in the region of the R/U instability. Fortunately, the effects of this instability diminish as correlation energy is introduced, and the RQCISD(T) curve is smooth. IRC curves such as these were calculated for all transition states connected to reactants or bimolecular products.

Note that the use of single-point energies obtained at geometries optimized with a different method often leads to an energy maximum along the IRC (labelled IRCmax) at a point other than the optimized transition state. For instance, the density functional theory (DFT) geometry of the transition state for hydrogen abstraction (**R** → **P1**) has an HO−$HC_2H$ distance of 1.062 Å, whereas the IRCmax at the RQCISD(T)/CBS level occurs somewhat earlier, at a distance of 1.158 Å. The difference in energy barriers (1.0 kcal/mol) is significant. When calculating rate coefficients variationally, it is the IRCmax value, rather than the energy barriers at the optimized geometries, that determines the low-temperature limit. The IRCmax, calculated at the RQCISD(T)/CBS//UB3LYP/6-311++G(d,p) level, are shown in Table 4 for those transition states treated variationally.

The Q1 diagnostics of Lee and co-workers[76,77] (labeled T1 in Gaussian[64] and Molpro[65] output files) are also shown in Tables 3 and 4 for the RQCISD(T) calculations. They suggest that several transition states contain significant multireference character. To assess the magnitude of the multideterminant effects, we performed multireference configuration−interaction (MRCI) calculations for the **R** → **P1**, **1** ↔ **2**, and **1** ↔ **P2** pathways, all of which have a substantial Q1 diagnostic (≥0.015) and play a significant role in the overall kinetics and/or product distribution. Specifically, we used the complete-active-space, self-consistent field (CASSCF) reference wave functions,[78,80] with singles and doubles CI excitations and Davidson corrections for quadruples excitations (MRCI+Q).[81,82] The basis-set extrapolation scheme mentioned previously was used in these MRCI+Q calculations, together with the UB3LYP/6-311++G(d,p) geometries. The forward and reverse energy barriers calculated with these methods are given in Table 5.

In the case of the hydrogen abstraction pathway, only the reverse process (i.e., **P1** → **R**) was studied with MRCI calculations. The active space consisted of nine electrons and nine orbitals: the $\sigma$ and $\sigma^*$ of both O−H bonds, the $\pi$ and $\pi^*$ of the C−C bond, and the $\sigma$ orbital on the $C_2H$ radical. The transition state for the isomerization reaction (**1** ↔ **2**) included seven electrons and six orbitals in the active space. These consisted of the $\sigma$ and $\sigma^*$ orbitals of C−H or O−H, the radical orbital on O or C, the $\pi$ and $\pi^*$ of the C−C bond, and a lone pair on O. Calculations of the decomposition to hydroxyacetylene (**1** ↔ **P2**) were performed with an active space of five electrons and five orbitals. These are the 1s orbital of the exiting H and the two perpendicular sets of $\pi$ and $\pi^*$ orbitals of the C−C bond. The inclusion of an O lone-pair in the active space had a negligible effect on the energies. In all transition states

**TABLE 5: Calculated Energy Barriers without Zero-Point Energy (ZPE), Extrapolated to the Complete Basis Set (CBS) Limit**

| | | calculated energy barrier without ZPE (kcal/mol) | | | | |
|---|---|---|---|---|---|---|
| | reaction | RHF | RQCISD(T) | CASSCF | MRCI | MRCI+Q |
| R → P1 | $C_2H_2 + OH \rightarrow C_2H + H_2O$ | 52.0 | 18.7 | | | |
| P1 → R | $C_2H + H_2O \rightarrow C_2H_2 + OH$ | 24.8 | 5.2 | 18.4 | 9.8 | 6.9 |
| 1 → 2 | $HOCHCH \rightarrow OCHCH_2$ | 54.3 | 38.4 | 45.2 | 41.4 | 39.0 |
| 2 → 1 | $OCHCH_2 \rightarrow HOCHCH$ | 80.5 | 65.5 | 74.6 | 69.1 | 66.2 |
| 1 → P2 | $HOCHCH \rightarrow H + HOCCH$ | 54.7 | 50.4 | 43.1 | 48.1 | 49.6 |
| P2 → 1 | $H + HOCCH \rightarrow HOCHCH$ | 9.3 | 2.0 | 8.1 | 4.4 | 3.0 |

studied, the occupancies of the CASSCF active orbitals were between 0.03 and 1.97.

The Davidson-corrected MRCI energy barriers are all within 1.6 kcal/mol of the RQCISD(T) values, providing us with considerable confidence in both estimates. It is likely that the uncertainties in these barriers are <2 kcal/mol. The comparatively large differences, up to 4.5 kcal/mol, between the MRCI calculations with and without the Davidson corrections suggests that the RQCISD(T) results are likely to be as reliable as the MRCI+Q results. Thus, the RQCISD(T) values are used in the kinetics calculations.

### III. Calculation of Rate Coefficients

Preliminary rate coefficient calculations demonstrated that the reaction flux leading to $H_2$ + HCCO (**P3** in Figure 1) was negligible; so, we eliminated this channel to simplify the analysis. Likewise, the formation of the cyclic intermediate $H(COC)H_2$ (**5**) is slow and was treated irreversibly as a bimolecular channel.

There are four conformers of complex **1**, shown in Figure 3. We note that, at the energies of interest, isomerization between these conformers is rapid relative to the time between collisions, resulting in fast microcanonical equilibration. Thus, internal rotations about the C−O bond (from **1a** to **1c** and from **1b** to **1d**) were simply considered to be hindered rotors for the purpose of calculating the density of states. The lowest-energy transformations for **1a** ↔ **1b** and **1c** ↔ **1d** involve a large-amplitude vibration with H atom motion in the CCO plane. These were treated harmonically, doubling the density of states of complex **1** to take into account the effect of the double-well potential. This approximation should be reasonably accurate, because the frequencies and energies of **1a** and **1b** are very similar, as are those of **1c** and **1d**.

The addition of OH to acetylene and the subsequent processes (i.e., stabilization, isomerization, and dissociation) were modeled with a multiple-well master equation (ME) of the form

$$\frac{dn_i(E)}{dt} = Z\int_{E_{0_i}}^{\infty} P(E \leftarrow E')n_i(E')\,dE' - Zn_i(E) - \sum_{j\neq i}^{4} k_{ji}(E)n_i(E) + \sum_{j\neq i}^{4} k_{ij}(E)n_j(E) - k_{\mathbf{P}_\alpha i}(E)n_i(E) + n_{\mathbf{R}}K_{\mathbf{R}i}^{eq}k_{\mathbf{R}i}(E)\frac{\rho_i(E)e^{-\beta E}}{Q_i(T)} - k_{\mathbf{R}i}(E)n_i(E) \qquad (\text{for } i = \mathbf{1}, ..., \mathbf{4}) \quad (7)$$

corresponding to the four stable species (**1** = HOCHCH, **2** = $OCHCH_2$, **3** = $HOCCH_2$, and **4** = $OCCH_3$). In eq 7, $n_i(E)$ is the population of complex $i$ at energy $E$, $E_{0_i}$ the ground-state energy of complex $i$, and $Z$ is the collision number per unit time. Collision rates were calculated using the Lennard-Jones potential parameters of ethanol[83] to represent the complexes. $P(E \leftarrow E')$ is the probability that a complex with an energy between $E'$ and $E' + dE'$ will be transferred by a collision to a state with an energy between $E$ and $E + dE$. Rates of collisional energy transfer (CET) for deactivating collisions were modeled using the "single exponential down" expression:

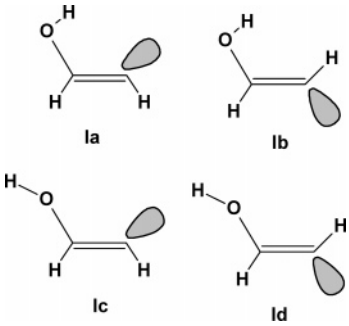


**Figure 3.** Conformers of isomer **1**.

$$P(E \leftarrow E') \propto \exp\left(-\frac{E' - E}{\langle \Delta E_d \rangle}\right) \qquad (\text{for } E' > E) \quad (8)$$

where $\langle \Delta E_d \rangle$ is an energy transfer parameter that depends on the nature of the collider gas. The value of $\langle \Delta E_d \rangle$ was determined as a function of temperature by fitting the data of Michael et al.[16] between 228 K and 413 K to a function with linear temperature dependence. CET rates for activating collisions were obtained from a detailed balance.

The term involving $k_{ji}(E)$ in eq 7 represents the rate of isomerization from $i$ to $j$, where $i,j = \{1, 2, 3, 4\}$ are the stable isomers (wells **1**−**4**), **R** the reactants (OH and $C_2H_2$), and $\mathbf{P}_\alpha$ a set of bimolecular products (**P1** = $H_2O + C_2H$, **P2** = H + HCCOH, **P4** = H + $CH_2CO$, **P5** = CO + $CH_3$, and **P6** = $H(COC)H_2$). Microcanonical rate coefficients were obtained from RRKM theory, and, in the case of dissociation transition states, these were calculated variationally. Asymmetric Eckart barriers were employed to compute the effect of tunneling through the reaction barriers.

To reduce the master equation to a linear form, we assume that the reaction takes place under pseudo-first-order conditions:

$$n_{OH} \ll n_{C_2H_2} \ll n_M \quad (9)$$

Solution of the master equation (ME) and the balance expression for $n_{OH}$,

$$\frac{dn_{OH}}{dt} = \int_{E_{0_1}}^{\infty} k_{\mathbf{R1}}(E)n_{\mathbf{1}}(E)\,dE - \frac{n_R}{Q_{\mathbf{1}}(T)}\int_{E_{01}}^{\infty} K_{\mathbf{R1}}^{eq}k_{\mathbf{R1}}(E)\rho_{\mathbf{1}}(E)e^{-\beta E}\,dE \quad (10)$$

was carried out by discretizing the energy and casting the system of equations as an eigenvalue problem. In eq 10, $\rho_{\mathbf{1}}(E)$ is the number of states of complex **1** with energy between $E$ and $E + dE$, and $Q_{\mathbf{1}}(T)$ is the corresponding canonical partition function. Rate coefficients were extracted from the solution eigenpairs, following the procedures described in refs 84−86. All rate coefficients were calculated with the VARIFLEX code.[87]

The analysis mentioned above describes the solution to a one-dimensional (1-d) ME with $E$ (the total energy) as the independent variable. Under certain conditions, it is straightforward to solve a two-dimensional (2-d) ME with $E$ and $J$ (the total angular momentum quantum number) as independent variables. The two conditions of interest here are the collisionless limit, obtained by setting $Z = 0$ in the two-dimensional analogue of eq 7,[88,89] and the irreversible dissociation of a single molecule (one well, but any number of dissociation channels).[90−92] In the latter case, rate coefficients for the association reaction are obtained from the reverse process by imposing detailed balance.[90−92]

Low-frequency torsional modes of intermediates and transition states were treated as hindered rotors. Torsional potentials were calculated at the B3LYP/6-311++G(d,p) level by varying the torsional angle while constraining the geometry of the rotating fragments. The resulting potentials were parametrized with the Fourier series,

$$V(\Delta\phi) = V_0 + \sum_{m=1} A_m \cos(m\Delta\phi) + \sum_{n=1} B_n \sin(n\Delta\phi) \quad (11)$$

The torsional parameters used, as well as Cartesian coordinates of some of the structures optimized, are given in the Supporting Information section. In all cases, six cosine terms plus four sine terms for asymmetric rotors were sufficient to obtain root mean square (RMS) fitting errors of $<1$ cm$^{-1}$. The Pitzer−Gwinn formalism[93] was used to account for quantum effects in the number and density of states functions, using the aforementioned potentials.

Spin−orbit interactions in OH cause a splitting of 126 cm$^{-1}$ between the $^2\Pi_{3/2}$ and $^2\Pi_{1/2}$ ground-state levels.[94] The ground-state OH radical at rest is described well as Hund's case (a) of angular momentum coupling. However, as the rotational quantum number increases, the spin angular momentum uncouples from the molecular-rotation axis, and the system quickly approaches case (b). In practice, this means that the splitting between the $J = {}^3/_2$ and $J = {}^1/_2$ levels of OH increases with the total angular momentum quantum number. Although spin uncoupling is significant in hydroxyl radicals, in the case of the addition transition state, this effect is expected to be negligible, because the coupling with the molecule's rotational axis is very weak. Thus, spin uncoupling was incorporated in the analysis by correcting the partition function of the reactants. Additional corrections were included to account for the fact that the Variflex code restricts the total angular momentum quantum number ($J$) to integer values when half-integer values are needed in the case of open-shell species. The combined correction factor for these two effects is 0.88 at room temperature and approaches unity as the temperature increases.

## IV. Results and Discussion

**A. High-Pressure Limit.** There has been some debate about the high-pressure limit of the rate coefficient ($k_\infty$) for the title reaction. Schmidt et al.[95] performed experiments with isotopically substituted reactants and confirmed that $O_2$ reacts with the collision complexes to regenerate OH. This implies that experiments measuring OH decay in the presence of oxygen would lead to decreased rate coefficients. In 1997, Fulle et al.[34] conducted experiments in helium at pressures up to 130 bar and temperatures close to room temperature. They found a value that was higher, by more than a factor of 2, than that found in previous experiments using air,[19,33] nitrogen,[23,24,27,33,96] and argon[15,16,18,22] diluents. A recent study by Sørensen and co-workers,[39] using two different methods to measure $C_2H_2$ decay to determine relative rate coefficients, confirmed the lower value. We used their recommended value of $k_\infty$ ($9.7 \times 10^{-13}$ cm$^3$ molecule$^{-1}$ s$^{-1}$ at 296 K) to calibrate our model. This resulted in the lowering of the entrance barrier by 1.1 kcal/mol. Such an adjustment is within the uncertainty of the ab initio calculations, especially given the large Q1 diagnostic for the association transition state. The calculated rate coefficient in the high-pressure limit is shown in Figure 4, along with those reported in previous studies.

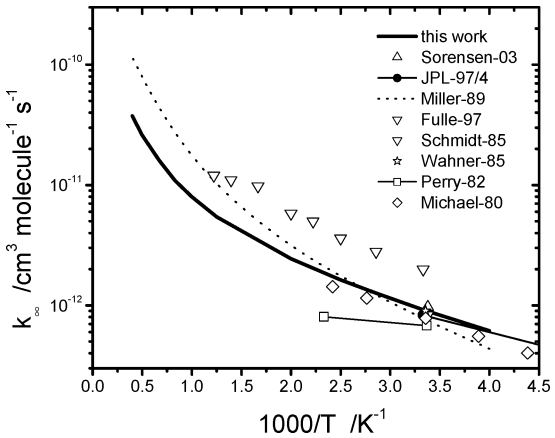


**Figure 4.** Calculated rate coefficients in the infinite pressure limit (solid line) and experimental data from previous studies.[16,18,22,23,34,35,39,40]

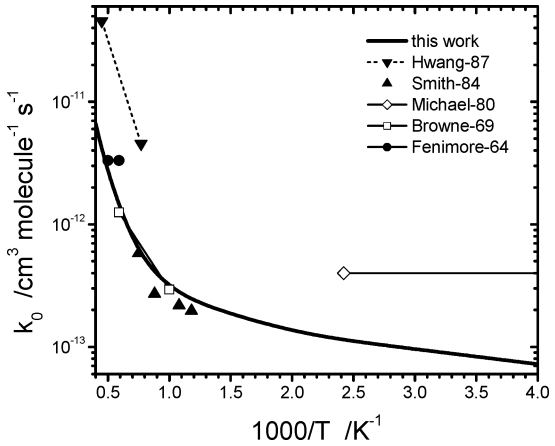


**Figure 5.** Total rate coefficients in the collisionless limit ($k_0$): this work (solid line) and experimental data.[7,8,16,21,25]

**B. Collisionless Limit and the Hydrogen Abstraction Channel.** Although there have been several measurements of the title reaction at temperatures of interest for combustion, most of these rate coefficients were derived indirectly, relying on an assumed reaction mechanism. The only direct measurements of the rate coefficients above 1200 K are the laser pyrolysis experiments by Smith, Fairchild, and Crosley[21] at low pressure and the pulse radiolysis experiments of Liu et al.[26] at atmospheric pressure. Rate coefficients in the zero-pressure limit ($k_0$) are shown in Figure 5, together with selected experimental data.[7,8,16,21,25] Our calculations in the collisionless limit (including hydrogen abstraction) agree well with the laser pyrolysis experiments of Smith et al.[21] and with the flame experiments of Fenimore and Jones[7] and Browne et al.[8]

Smith et al.[21] attributed the increase in activation energy they observed above 1200 K to the hydrogen abstraction channel ($k_1$). Our calculations show an increase in the rate coefficients

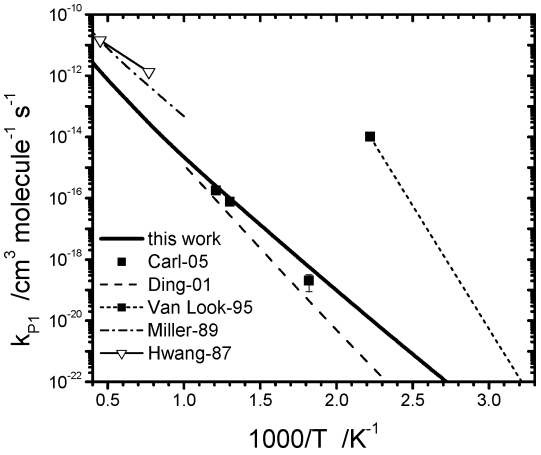


**Figure 6.** Rate coefficients for the direct abstraction reaction ($k_1$) channel from the present calculations (dashed line) and from previous studies.[25,40] Also shown are rate coefficients obtained from our calculated equilibrium constants and data from studies of the reverse reaction.[41,42,97]

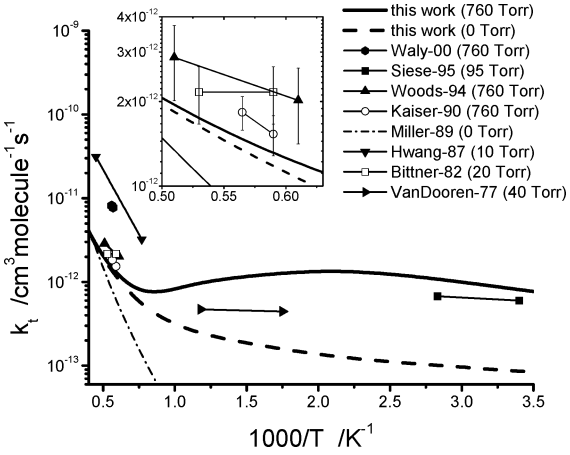


**Figure 7.** Total rate coefficients without the hydrogen abstraction channel ($k_t$). Calculations at 1 atm of argon are depicted with a solid line and those in the collisionless limit with a dashed line. Also shown are $k_t$ values from previous experimental[6,14,17,25,29,32,36] and theoretical[40] studies.

leading to **P2** and **P1** channels above 1200 K. This is caused by the opening of entropically favored transition states, namely **1** → **P2** and **R** → **P1**. The effect of the 1,2-hydrogen shift (**1** ↔ **3**) was determined to be unimportant below 2000 K.

Our hydrogen abstraction rate coefficients, shown in Figure 6, are noticeably smaller than those obtained in previous studies.[25,40] The difference is largely due to a significantly higher energy barrier used in the present study, based on the ab initio calculations. The fact that the MRCI+Q calculations yielded an even higher barrier for this channel (+19.7 kcal/mol) suggests that the calculated $k_1$ can be regarded, more or less, as an upper limit. Variational effects in the hydrogen abstraction channel were found to be unimportant; e.g., they decrease the rate coefficient by only 4% at 2000 K.

The reverse hydrogen abstraction reaction has been studied theoretically by Ding et al.[41] and experimentally by Van Look and Peeters[97] and, more recently, by Carl et al.[42] In this re-examination by the Peeters group, the authors concluded that the rate coefficients reported in ref 97 were too high, probably due to incomplete mixing. Rate coefficients ($k_1$) for the hydrogen abstraction channel, derived from the reverse reaction[41,97] and our calculated equilibrium constants, are also shown in Figure 6. Our calculated rate coefficients agree well with those computed by Ding and co-workers[41] and the newer measurements from the Peeters group;[42] however, they are incompatible by several orders of magnitude with the older measurements by Van Look and Peeters in the temperature range of 295−450 K.[97]

It is important to note that Evans−Polanyi-type correlations suggest that the activation energy for the (reverse) hydrogen abstraction reaction should be higher than that for $C_2H + H_2$, i.e., ≥ 2.5 kcal/mol. Our calculated reverse barrier of 5.2 kcal/mol, as well as those calculated by Ding et al. (5.5 kcal/mol)[41] and Carl et al. (4.1 kcal/mol),[42] satisfy this empirical rule, while the barrier used in ref 40 and the activation energies derived from refs 25 and 97 are considerably smaller.

The effect of conserving total angular momentum was studied by solving the 2d master equation ($E$, $J$ resolved) in the collisionless limit,[88,89] where rotational effects are expected to be the largest. At intermediate and high temperatures, the rate coefficients calculated with the 1d and the 2d master equations are similar. For example, at 300 K, the $J$-conserved rate coefficient (in the collisionless limit) is 88% of that obtained from the 1d master equation, and the difference between the two diminishes at higher temperatures.

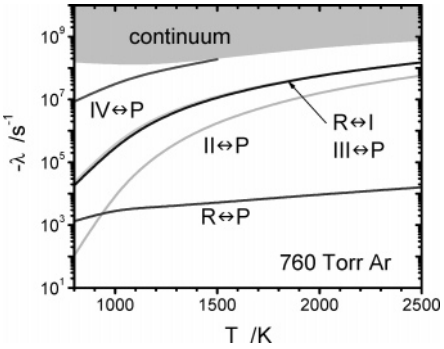


**Figure 8.** Eigenvalues of the master equations for $P = 760$ Torr and $P_{C_2H_2} = 1$ Torr. The quasi-continuum of eigenvalues corresponding to internal energy relaxation is shown in gray.

In Figure 7, we compare our total rate coefficient for all channels except the hydrogen abstraction ($k_t$) with experiments reporting rate coefficients for channels other than the hydrogen abstraction.[6,14,17,25,29,32,36] At combustion temperatures, our results for $k_t$ are in remarkably good agreement with the experiments of Woods and Haynes,[6] Kaiser,[29] and Bittner and Howard,[17] who all measured hydrocarbon concentrations at conditions where the hydrogen abstraction reaction is essentially equilibrated. The rate coefficients proposed by Waly et al.[37] and Hwang et al.[25] for the ketene channel are about five times as large as our calculations and previous measurements of $k_t$ in this temperature range.[6,17,29] The previous theoretical study of Miller and Melius[40] underpredicts $k_t$ at lower temperatures. Measurements at lower temperatures by Vandooren and Van Tiggelen[14] and by Siese and Zetzsch[32] are not in the collisionless limit and lie between our calculations at 0 and 760 Torr.

**C. Pressure Dependence.** Eigenvalues resulting from the solution of the master equation system at 760 Torr are shown in Figure 8. Those corresponding to internal energy relaxation modes form a quasi-continuum, which is depicted with gray shading in the figure. In this case, the five smallest (least negative) eigenvalues are "chemically significant". Each of these characterizes the rate of equilibration of two (or more) chemical species. Except at low temperatures and pressures, the smallest (least-negative) eigenvalue corresponds to the equilibration

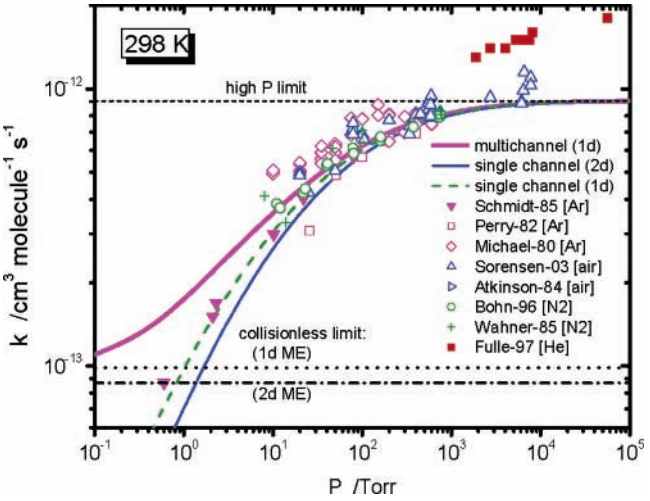


**Figure 9.** Rate coefficient at 298 K as a function of pressure. Present calculations were done using an argon bath gas, with a multichannel 1d master equation (thick solid line), a single channel 2d master equation (thin solid line) and a single channel 1d master equation (dashed line). Also indicated are the high-pressure limit (short dashed line) and collisionless limits obtained from 1d and 2d master equations (dotted and dash−dotted lines, respectively). For comparison, experimental measurements using argon,[16,18,22] air,[19,39] nitrogen,[23,33] and helium[34] colliding partners are shown.

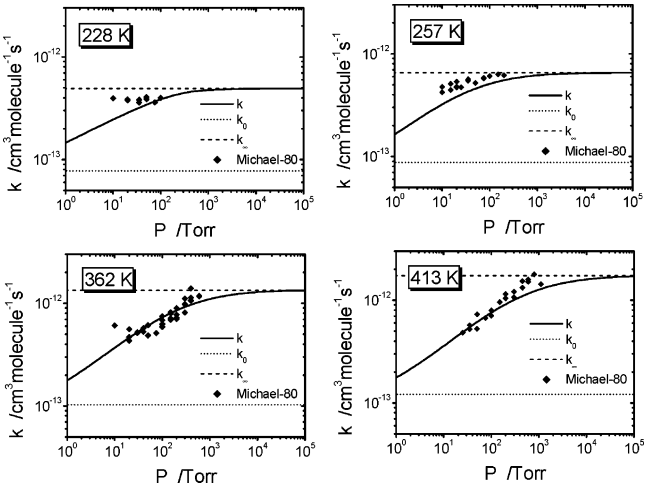


**Figure 10.** Rate coefficients as a function of pressure at 228, 257, 362, and 413 K: (—) calculated rate coefficient, (- - -) high-pressure limit, and (• • •) low-pressure limit. Experimental data[16] are represented by symbols.

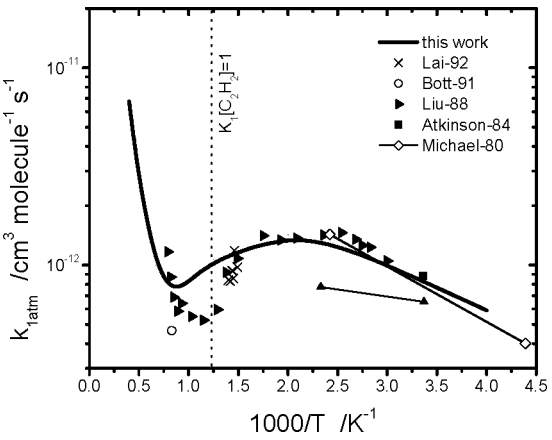


**Figure 11.** Calculated rate coefficients at 1 atm of argon (solid line) and experimental data.[16,19,26,30,31]

between reactants and bimolecular products. The transition state connecting well **4** to products is so low in energy that the eigenvalue corresponding to this transition state enters the quasi-continuum region at a temperature just above 1500 K. This implies that the thermal dissociation of $CH_3CO$ to $CH_3 + CO$ occurs completely as part of the vibrational relaxation process above this temperature.

There have been several studies that measured the pressure dependence of the overall reaction near room temperature using helium,[34] air,[39] nitrogen,[23,33] and argon[16,18] bath gases. We fit the data of Michael et al.[16] in the 228−413 K range to obtain the collisional energy transfer parameter $\langle \Delta E_d \rangle = 160\ \text{cm}^{-1}(T/300\ \text{K})$ with an argon collider. We note that this fit is rather approximate given the scatter in the experimental data and the form of the temperature dependence is solely empirical, based on those obtained for similar systems.[90,98]

Figure 9 shows the rate coefficients at 298 K, calculated with a multichannel, 1d master equation (thick solid line), a single channel 2d master equation (thin solid line), and a single-channel, 1d master equation (dashed line). At pressures above 10 Torr, the difference between the rate coefficients obtained from the 1d and 2d master equations is small, well within the scatter of the experimental data. Below this pressure, contributions from channels other than intermediate stabilization are important. The effect of conserving total angular momentum is small at 1 Torr and negligible at pressures higher than 10 Torr. At 300 K, the collisionless rate coefficients obtained from the 1d master equation are 14% larger than those obtained with the 2d form. Also shown in Figure 9 are the rate coefficients in the high-pressure limit, calculated with transition state theory (short dash line) and those at the collisionless limit, obtained from 1d and 2d master equations (dotted and dash−dotted lines, respectively).

Fall-off curves at other temperatures are shown in Figure 10, along with experimental data from Michael et al.[16] At temperatures of below 250 K and low pressures, the eigenvalue method for obtaining rate coefficients incurred numerical problems, so eqs 2 and 5 were integrated numerically with an ordinary differential equation (ODE) solver.[99] The value of $\langle \Delta E_d \rangle$ used results in a good fit to all the data, even at the lowest temperature where the experiments do not show any pressure dependence.

While the study of Michael et al.[16] reported a temperature-independent value of $4 \times 10^{-13}$ cm$^3$ molecule$^{-1}$ s$^{-1}$ for the rate coefficients extrapolated to the limit of zero pressure, Perry and Williamson[18] observed no appreciable zero-pressure intercept. Our rate coefficients decrease monotonically with pressure and agree well with the low-pressure measurements of Schmidt et al.,[22] suggesting that the zero-pressure intercept reported in ref 16 is too high. We note that our calculated zero-pressure limit at room temperature ($8.8 \times 10^{-14}$ cm$^3$ molecule$^{-1}$ s$^{-1}$) may be below the detection limit of ref 18.

Calculated rate coefficients in 1 atm of argon are shown in Figure 11, along with several experimental values.[16,19,26,30,31] Agreement with experiment is good except at intermediate temperatures (700 K < $T$ < 1200 K), where our calculations are higher than the experimental values by factors up to 1.8. In this temperature range, the pseudo-first-order forward and reverse reaction rate coefficients are approximately equal (i.e., $K_{\mathbf{R1}}^{\text{eq}} \times [C_2H_2] \approx 1$). It is not clear whether or not the dissociation of the addition complex (**1**) back to reactants was considered in the fit of OH decay in ref 26. If it was not

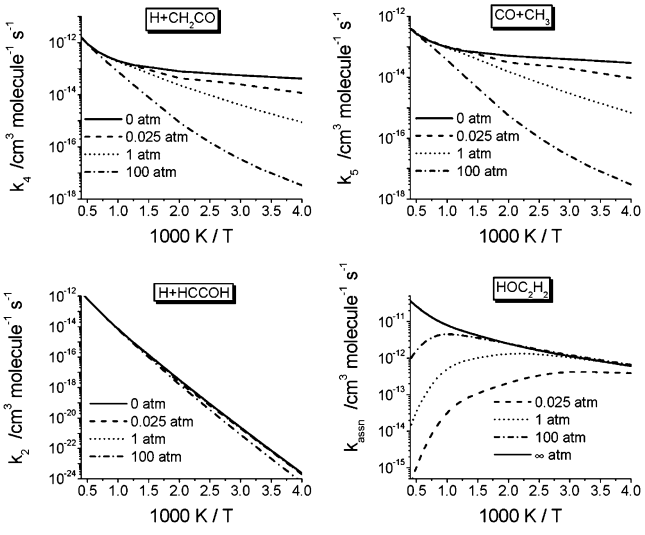


**Figure 12.** Calculated rate coefficients for association of OH and $C_2H_2$ and reactions leading to H + $CH_2CO$, $CH_3$ + CO, and H + HCCOH at several pressures.

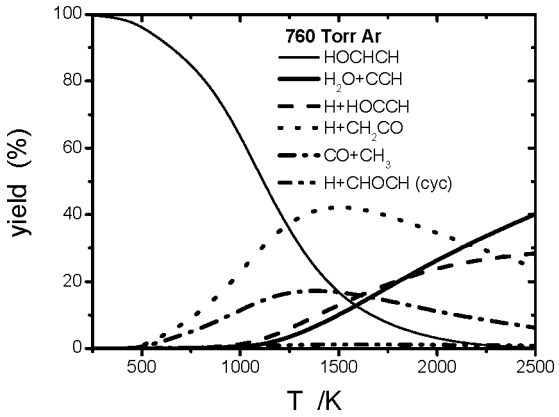


**Figure 13.** Calculated product branching in 1 atm of argon bath gas, as a function of temperature. Products are HOCHCH (thick solid line), $H_2O$ + $C_2H$ (thin solid line), H + HOCCH (dashed line), H + $CH_2CO$ (dotted line), CO + $CH_3$ (dash−dotted line), and H + H(COC)H (dash−dot-dot line).

(probably the case), their analysis would have resulted in an underestimation of the rate coefficient, explaining the difference between our calculations and the experimental data. We stress that our rate coefficients account for this equilibration process and are derived *unambiguously* from the theoretical formalism presented previously.

**D. Branching Ratios.** Figure 12 shows Arrhenius plots for the **P4**, **P5**, **P2**, and association channels at several pressures. The rate coefficient for association ($k_{assn}$) shows a strong pressure dependence and decreases with increasing temperature at all but the highest pressures. This is caused by a proportional increase of activating collisions, relative to deactivating ones at higher temperatures, as well as by an enhancement of the dissociation back to reactants. Competition between isomerization and dissociation reactions with collisional stabilization causes $k_4$, $k_5$, and, to a lesser extent, $k_2$ to decrease at low temperatures as the pressure is increased. The higher barrier for the **P2** channel is responsible for the decreased pressure sensitivity.

Product branching ratios as a function of temperature are shown in Figures 13 and 14 (in 1 atm of argon in Figure 13 and in the collisionless limit in Figure 14). At 1 atm and

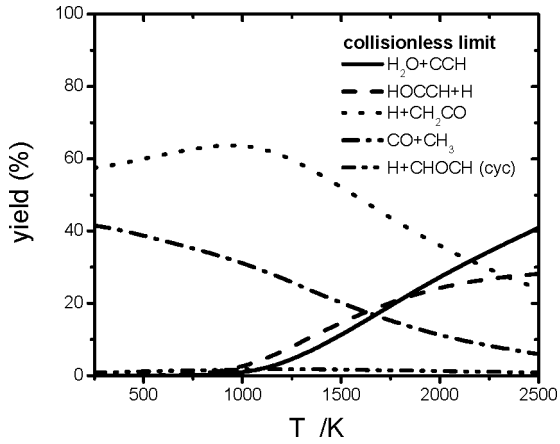


**Figure 14.** Calculated product branching in the collisionless limit as a function of temperature. Products are $H_2O$ + $C_2H$ (thin solid line), H + HOCCH (dashed line), H + $CH_2CO$ (dotted line), CO + $CH_3$ (dash−dotted line), and H + H(COC)H (dash−dot-dot line).

temperatures below 1250 K, complex **1** is the main product, because the energy barriers for isomerization and hydrogen abstraction are considerably higher than the association barrier. In fact, there is never significant stabilization into any of the other wells, even at higher pressures. As the temperature is increased, back dissociation from **1** to reactants prior to stabilization, as well as isomerization and decomposition to H + $CH_2CO$ and CO + $CH_3$ products, becomes important. Thus, production of ketene is the main channel at temperatures between 1200 and 2100 K and atmospheric pressure. Eventually, flux through entropically favored transition states becomes significant, leading to higher yields of HOCCH and $C_2H$ at high temperatures.

Our calculations show that the channel leading to hydroxyacetylene is not as important as previously thought,[40] being surpassed by H + $CH_2CO$ and CO + $CH_3$ at low temperatures and by direct abstraction at higher temperatures.

## V. Concluding Remarks

Calculations in the present investigation are based entirely on the ab initio potential energy surface, except for a minor adjustment to the association energy barrier. Overall agreement with experimental assessments is good, considering the discrepancies in the experimental data.

The most significant differences between the present analysis and the previous theoretical work of Miller and Melius[40] are a smaller rate coefficient for the direct abstraction channel (which accounts for only ∼11% of the total rate coefficient at 1500 K and zero pressure) and the predominance of the ketene product channel at temperatures below 2100 K in the present work. At atmospheric pressure, channels **P4** (H + ketene) and **P5** ($CH_3$ + CO) compete with the stabilization of complex **1**. Calculations at low temperatures indicate a collisionless-limit rate coefficient smaller than the constant value found by Michael et al.,[16] but higher than that predicted in ref 40, with $k_0/k_\infty \approx 9.1\%$ at room temperature in the present work.

Rate coefficient expressions for use in modeling are summarized in Table 6.

**Supporting Information Available:** Torsional parameters used, as well as Cartesian coordinates of some of the structures optimized (PDF). This material is available free of charge via the Internet at http://pubs.acs.org.

**TABLE 6: Parametric Fits of Calculated Rate Coefficients at Several Pressures of Ar Diluent**

| | channel | pressure, $P$ (atm) | $A$ | $B$ | $C$ | $D$ | $E$ | $F$ |
|---|---|---|---|---|---|---|---|---|
| **P1** | $H_2O + C_2H$[a,b] | | $4.37 \times 10^{-18}$ | 2.14 | 8586 | | | |
| **P2** | $HCCOH + H$[b] | 0 | $5.88 \times 10^{-18}$ | 1.95 | 6369 | | | |
| | | 0.01 | $4.65 \times 10^{-19}$ | 2.28 | 6250 | | | |
| | | 0.025 | $1.24 \times 10^{-18}$ | 2.16 | 6315 | | | |
| | | 0.1 | $2.95 \times 10^{-18}$ | 2.04 | 6376 | | | |
| | | 1 | $4.01 \times 10^{-18}$ | 2.00 | 6398 | | | |
| | | 10 | $5.33 \times 10^{-18}$ | 1.97 | 6447 | | | |
| | | 100 | $1.22 \times 10^{-17}$ | 1.89 | 6846 | | | |
| **P4** | $CH_2CO + H$[b] | 0 | $4.49 \times 10^{-21}$ | 2.47 | −636 | | | |
| | | 0.01 | $2.62 \times 10^{-21}$ | 2.56 | −425 | | | |
| | | 0.025 | $2.52 \times 10^{-20}$ | 2.28 | −147 | | | |
| | | 0.1 | $5.01 \times 10^{-19}$ | 1.92 | 301 | | | |
| | | 1 | $1.25 \times 10^{-17}$ | 1.55 | 1060 | | | |
| | | 10 | $8.47 \times 10^{-18}$ | 1.65 | 1711 | | | |
| | | 100 | $2.42 \times 10^{-20}$ | 2.45 | 2253 | | | |
| **P5** | $CO + CH_3$[b] | 0 | $1.02 \times 10^{-18}$ | 1.62 | −368 | | | |
| | | 0.01 | $7.90 \times 10^{-19}$ | 1.68 | −166 | | | |
| | | 0.025 | $7.26 \times 10^{-18}$ | 1.40 | 114 | | | |
| | | 0.1 | $1.27 \times 10^{-16}$ | 1.05 | 561 | | | |
| | | 1 | $2.12 \times 10^{-15}$ | 0.73 | 1298 | | | |
| | | 10 | $7.16 \times 10^{-16}$ | 0.92 | 1880 | | | |
| | | 100 | $1.37 \times 10^{-18}$ | 1.77 | 2364 | | | |
| **1** | $HOC_2H_2$[c] | 0.01 | $4.77 \times 10^{+40}$ | −18.57 | 5037 | $4.38 \times 10^{+09}$ | −7.36 | 3217 |
| | | 0.025 | $7.79 \times 10^{+35}$ | −16.87 | 4573 | $7.27 \times 10^{+08}$ | −7.02 | 2986 |
| | | 0.1 | $2.06 \times 10^{+04}$ | −5.56 | 1874 | $1.06 \times 10^{+19}$ | −9.96 | 5907 |
| | | 1 | $3.16 \times 10^{+20}$ | −11.38 | 3170 | $5.79 \times 10^{+07}$ | −6.20 | 3339 |
| | | 10 | $2.47 \times 10^{+00}$ | −4.06 | 1641 | $7.48 \times 10^{+07}$ | −5.92 | 4409 |
| | | 100 | $1.03 \times 10^{-03}$ | −2.80 | 1425 | $2.66 \times 10^{+05}$ | −4.91 | 4899 |
| | | ∞ | $1.80 \times 10^{-16}$ | 1.34 | 167 | $1.00 \times 10^{-16}$ | 1.62 | 121 |

[a] Hydrogen abstraction channel is independent of pressure. [b] $k(T) = AT^B \exp(-C/T)$. Units for $k(T)$ are cm$^3$ molecule$^{-1}$ s$^{-1}$, and temperature is given in Kelvin (K). [c] $k(T) = AT^B \exp(-C/T) + DT^E \exp(-F/T)$. Units for $k(T)$ are cm$^3$ molecule$^{-1}$ s$^{-1}$, and temperature is given in Kelvin (K).

**Acknowledgment.** This work was supported by the United States Department of Energy, Office of Basic Sciences, Division of Chemical Sciences, Geosciences and Biosciences. Sandia is a multiprogram laboratory operated by Sandia Corporation, a Lockheed Martin Company, for the United States Department of Energy's National Nuclear Security Administration, under Contract No. DE-AC04-94AL85000.

## References and Notes

(1) Lindstedt, R. P.; Skevis, G. *Combust. Sci. Technol.* **1997**, *125*, 73−137.
(2) Seinfeld, J. H. *Atmospheric Chemistry and Physics of Air Pollution*; Wiley: New York, 1986.
(3) Moses, J. I.; Lellouch, E.; Bezard, B.; Gladstone, G. R.; Feuchtgruber, H.; Allen, M. *Icarus* **2000**, *145*, 166−202.
(4) Miller, J. A.; Kee, R. J.; Westbrook, C. K. *Annu. Rev. Phys. Chem.* **1990**, *41*, 345−387.
(5) Miller, J. A.; Melius, C. F. *Combust. Flame* **1992**, *91*, 21−39.
(6) Woods, I. T.; Haynes, B. S. *Proc. Combust. Inst.* **1994**, *25*, 909−917.
(7) Fenimore, C. P.; Jones, G. W. *J. Chem. Phys.* **1964**, *41*, 1887−1889.
(8) Browne, W. G.; Porter, R. P.; Verlin, J. D.; Clark, A. H. *Proc. Combust. Inst.* **1968**, *12*, 1035−1047.
(9) Bradley, J. N. T., R. S. *J. Chem. Soc., Faraday Trans.* **1969**, *65*, 2685−2692.
(10) Breen, J. E.; Glass, G. P. *Int. J. Chem. Kinet.* **1970**, *3*, 145.
(11) Smith, I. W. M.; Zellner, R. *J. Chem. Soc., Faraday Trans. 2* **1973**, *69*, 1617.
(12) Pastrana, A.; Carr, R. W. *Ber. Bunsen.−Ges.* **1974**, *78*, 204.
(13) Davis, D. D.; Fischer, S.; Schiff, R.; Watson, R. T.; Bollinger, W. *J. Chem. Phys.* **1975**, *63*, 1707−1712.
(14) Vandooren, J.; Van Tiggelen, P. J. *Proc. Combust. Inst.* **1976**, *16*, 1133−1144.
(15) Perry, R. A.; Atkinson, R.; Pitts, J. N. *J. Chem. Phys.* **1977**, *67*, 5577−5584.
(16) Michael, J. V.; Nava, D. F.; Borkowski, R. P.; Payne, W. A.; Stief, L. J. *J. Chem. Phys.* **1980**, *73*, 6108−6116.
(17) Bittner, J. D.; Howard, J. B. *Proc. Combust. Inst.* **1982**, *19*, 211.
(18) Perry, R. A.; Williamson, D. *Chem. Phys. Lett.* **1982**, *93*, 331−334.
(19) Atkinson, R.; Aschmann, S. M. *Int. J. Chem. Kinet.* **1984**, *16*, 259−268.
(20) Fairchild, P. W.; Smith, G. P.; Crosley, D. R. Reaction rate of OH and $C_2H_2$ near 1100 kelvin. In *The Chemistry of Combustion Processes*; ACS Symposium Series, Vol. 249; American Chemical Society: Washington, DC, 1984; pp 239−256.
(21) Smith, G. P.; Fairchild, P. W.; Crosley, D. R. *J. Chem. Phys.* **1984**, *81*, 2667−2677.
(22) Schmidt, V.; Zhu, G. Y.; Becker, K. H.; Fink, E. H. *Ber. Bunsen.−Ges.* **1985**, *89*, 321−322.
(23) Wahner, A.; Zetzsch, C. *Ber. Bunsen.−Ges.* **1985**, *89*, 323−325.
(24) Klopffer, W.; Frank, R.; Kohl, E. G.; Haag, F. *Chem.−Ztg.* **1986**, *110*, 57−61.
(25) Hwang, S. M.; Gardiner, W. C.; Frenklach, M.; Hidaka, Y. *Combust. Flame* **1987**, *67*, 65−75.
(26) Liu, A. D.; Mulac, W. A.; Jonah, C. D. *J. Phys. Chem.* **1988**, *92*, 5942−5945.
(27) Arnts, R. R.; Seila, R. L.; Bufalini, J. J. *J. Air Waste Manage.* **1989**, *39*, 453−460.
(28) Liu, A. D.; Jonah, C. D.; Mulac, W. A. *Radiat. Phys. Chem.* **1989**, *34*, 687−691.
(29) Kaiser, E. W. *J. Phys. Chem.* **1990**, *94*, 4493−4499.
(30) Bott, J. F.; Cohen, N. *Int. J. Chem. Kinet.* **1991**, *23*, 1075−1094.
(31) Lai, L. H.; Hsu, Y. C.; Lee, Y. P. *J. Chem. Phys.* **1992**, *97*, 3092−3099.
(32) Siese, M.; Zetzsch, C. *Z. Phys. Chem.−Int. J. Res. Phys. Chem., Chem. Phys.* **1995**, *188*, 75−89.
(33) Bohn, B.; Siese, M.; Zetzsch, C. *J. Chem. Soc., Faraday Trans.* **1996**, *92*, 1459−1466.
(34) Fulle, D.; Hamann, H.; Hippler, H.; Jansch, C. *Ber. Bunsen.−Ges.* **1997**, *101*, 1433−1442.
(35) DeMore, W.; Bayes, K. *J. Phys. Chem. A* **1999**, *103*, 2649−2654.
(36) Waly, M. M. Y.; Li, S. C.; Williams, F. A. *J. Eng. Gas Turbines Power* **2000**, *122*, 651−658.
(37) Waly, M. M. Y.; Li, S. C.; Williams, F. A. *Proc. Combust. Inst.* **2000**, *28*, 2005−2012.
(38) Lee, J.; Bozzelli, J. W. *Int. J. Chem. Kinet.* **2003**, *35*, 20−44.
(39) Sørensen, M.; Kaiser, E.; Hurley, M.; Wallington, T.; Nielsen, O. *Int. J. Chem. Kinet.* **2003**, *35*, 191−197.

(40) Miller, J. A.; Melius, C. F. *Proc. Combust. Inst.* **1988**, *22*, 1031−1039.
(41) Ding, Y.; Zhang, X.; Li, Z.; Huang, X.; Sun, C. *J. Phys. Chem. A* **2001**, *105*, 8206−8215.
(42) Carl, S. A.; Nguyen, H. M. T.; Elsamra, R. I.; Nguyen, M. T.; Peeters, J. *J. Chem. Phys.* **2005**, *122*, 114307.
(43) Dupuis, M.; Wendoloski, J. J.; Lester, W. A. *J. Chem. Phys.* **1982**, *76*, 488−492.
(44) Huyser, E. S.; Feller, D.; Borden, W. T.; Davidson, E. R. *J. Am. Chem. Soc.* **1982**, *104*, 2956−2959.
(45) Sosa, C.; Schlegel, H. B. *J. Am. Chem. Soc.* **1987**, *109*, 4193−4198.
(46) Bauschlicher, C. W. *J. Phys. Chem.* **1994**, *98*, 2564−2566.
(47) Dolgounitcheva, O.; Zakrzewski, V.; Ortiz, J. *J. Phys. Chem. A* **1997**, *101*, 1758−1762.
(48) Osborn, D.; Choi, H.; Mordaunt, D.; Bise, R.; Neumark, D.; Rohlfing, C. *J. Chem. Phys.* **1997**, *106*, 3049−3066.
(49) Mao, W.; Li, Q.; Kong, F.; Huang, M. *Chem. Phys. Lett.* **1998**, *283*, 114−118.
(50) Alconcel, L. S.; Deyerl, H. J.; Zengin, V.; Continetti, R. E. *J. Phys. Chem. A* **1999**, *103*, 9190−9194.
(51) Bouchoux, G.; Chamot-Rooke, J.; Leblanc, D.; Mourgues, P.; Sablier, M.; *ChemPhysChem* **2001**, *2*, 235−241.
(52) Davey, J. B.; Greenslade, M. E.; Marshall, M. D.; Lester, M. I.; Wheeler, M. D.; *J. Chem. Phys.* **2004**, *121*, 3009−3018.
(53) Bencsura, A.; Knyazev, V. D.; Slagle, I. R.; Gutman, D.; Tsang, W. *Ber. Bunsen.−Ges.* **1992**, *96*, 1338−1347.
(54) Mordaunt, D.; Osborn, D.; Neumark, D. *J. Chem. Phys.* **1998**, *108*, 2448−2457.
(55) Peña-Gallego, A.; Martínez-Núñez, E.; Vázquez, S. A. *J. Chem. Phys.* **1999**, *110*, 11323−11334.
(56) Lee, J.; Chen, C.; Bozzelli, J. *J. Phys. Chem. A* **2002**, *106*, 7155−7170.
(57) Matsika, S.; Yarkony, D. *J. Chem. Phys.* **2002**, *117*, 7198−7206.
(58) Morokuma, K.; Khoroshun, D. *Am. Chem. Soc. [Proc.]* **2002**, *223*, U497.
(59) Becke, A. *Phys. Rev. A* **1988**, *38*, 3098−3100.
(60) Stephens, P. J.; Devlin, F. J.; Chabalowski, C. F.; Frisch, M. J. *J. Phys. Chem.* **1994**, *98*, 11623−11627.
(61) Baboul, A. G.; Curtiss, L. A.; Redfern, P. C.; Raghavachari, K. *J. Chem. Phys.* **1999**, *110*, 7650−7657.
(62) Halls, M. D.; Velkovski, J.; Schlegel, H. B. *Theor. Chem. Acc.* **2001**, *105*, 413−421.
(63) Hampel, C.; Peterson, K. A.; Werner, H.-J. *Chem. Phys. Lett.* **1992**, *190*, 1−12.
(64) Frisch, M. J.; Trucks, G. W.; Schlegel, H. B.; Scuseria, G. E.; Robb, M. A.; Cheeseman, J. R.; Zakrzewski, V. G.; Montgomery, J. A., Jr.; Stratmann, R. E.; Burant, J. C.; Dapprich, S.; Millam, J. M.; Daniels, A. D.; Kudin, K. N.; Strain, M. C.; Farkas, O.; Tomasi, J.; Barone, V.; Cossi, M.; Cammi, R.; Mennucci, B.; Pomelli, C.; Adamo, C.; Clifford, S.; Ochterski, J.; Petersson, G. A.; Ayala, P. Y.; Cui, Q.; Morokuma, K.; Malick, D. K.; Rabuck, A. D.; Raghavachari, K.; Foresman, J. B.; Cioslowski, J.; Ortiz, J. V.; Stefanov, B. B.; Liu, G.; Liashenko, A.; Piskorz, P.; Komaromi, I.; Gomperts, R.; Martin, R. L.; Fox, D. J.; Keith, T.; Al-Laham, M. A.; Peng, C. Y.; Nanayakkara, A.; Gonzalez, C.; Challacombe, M.; Gill, P. M. W.; Johnson, B. G.; Chen, W.; Wong, M. W.; Andres, J. L.; Head-Gordon, M.; Replogle, E. S.; Pople, J. A. *Gaussian 98*, revision A.7; Gaussian, Inc.: Pittsburgh, PA, 1998.
(65) Werner, H.-J.; Knowles, P. J.; Amös, R. D.; Bernhardsson, A.; Berning, A.; Celani, P.; Cooper, D. L.; Deegan, M. J. O.; Doobbyn, A. J.; Eckert, F.; Hampel, C.; Hetzer, G.; Korona, T.; Lindh, R.; Lloyd, A. W.; McNicholas, S. J.; Manby, F. R.; Meyer, W.; Mura, M. E.; Nicklass, A.; Palmieri, P.; Pitzer, R.; Rauhut, G.; Schütz, M.; Schumann, U.; Stroll, H.; Stone, A. J.; Tarroni, R.; Thorsteinsson, T. MOLPRO, Version 2002.1 Edition, 1998. (MOLPRO is a package of ab initio programs.)
(66) Martin, J. M. L. *Chem. Phys. Lett.* **1996**, *259*, 669−678.
(67) Feller, D.; Dixon, D. A. *J. Chem. Phys.* **2001**, *115*, 3484−3496.
(68) In the limit of an infinite basis set, the basis set superposition error (BSSE) is zero.
(69) Mayer, P. M.; Parkinson, C. J.; Smith, D. M.; Radom, L. *J. Chem. Phys.* **1998**, *108*, 604−615.
(70) Møller, C.; Plesset, M. S. *Phys. Rev.* **1934**, *46*, 618−622.
(71) Greenwald, E. E.; North, S.; Georgievskii, Y.; Klippenstein, S. J. *J. Phys. Chem. A* **2005**, *109*, 6031−6044.
(72) Singleton, D. L.; Cvetanoviç, R. J. *J. Am. Chem. Soc.* **1976**, *98*, 6812−6819.
(73) Benson, S. W.; Dobis, O. *J. Phys. Chem. A* **1998**, *102*, 5175−5181.
(74) Alvarez-Idaboy, J. R.; Mora-Diez, N.; Vivier-Bunge, A. *J. Am. Chem. Soc.* **2000**, *122*, 3715−3720.
(75) Smith, I. W. M.; Ravishankara, A. R. *J. Phys. Chem. A* **2002**, *106*, 4798−4807.
(76) Lee, T. J.; Taylor, P. R. *Int. J. Quantum Chem., Quantum Chem. Symp.* **1989**, *23*, 199−207.
(77) Lee, T. J.; Rendell, A. P.; Taylor, P. R. *J. Phys. Chem.* **1990**, *94*, 5463−5468.
(78) Roos, B. O.; Taylor, P. R.; Siegbahn, P. E. M. *Chem. Phys.* **1980**, *48*, 157−173.
(79) Knowles, P. J.; Werner, H.-J. *Chem. Phys. Lett.* **1985**, *115*, 259−267.
(80) Werner, H.-J.; Knowles, P. J. *J. Chem. Phys.* **1985**, *82*, 5053−5063.
(81) Knowles, P. J.; Werner, H.-J. *Chem. Phys. Lett.* **1988**, *145*, 514−522.
(82) Werner, H.-J.; Knowles, P. J. *J. Chem. Phys.* **1988**, *89*, 5803−5814.
(83) Poling, B. E.; Prausnitz, J. M.; O'Connell, J. P. *The Properties of Gases and Liquids*, 5th Edition; McGraw-Hill: New York, 2001.
(84) Miller, J. A.; Klippenstein, S. J.; Robertson, S. H. *J. Phys. Chem. A* **2000**, *104*, 7525−7536. See also, *J. Phys. Chem. A* **2000**, *104*, 9806 (correction).
(85) Klippenstein, S. J.; Miller, J. A. *J. Phys. Chem. A* **2002**, *106*, 9267−9277.
(86) Miller, J. A.; Klippenstein, S. J. *J. Phys. Chem. A* **2003**, *107*, 2680−2692.
(87) Klippenstein, S. J.; Wagner, A. F.; Dunbar, R. C.; Wardlaw, D. M.; Robertson, S. H.; Miller, J. A., VARIFLEX, Version 1.13m, 2003.
(88) Miller, J. A.; Parrish, C.; Brown, N. J. *J. Phys. Chem.* **1986**, *90*, 3339−3345.
(89) Hahn, D. K.; Klippenstein, S. J.; Miller, J. A. *Faraday Discuss.* **2001**, *119*, 79−100.
(90) Miller, J. A.; Klippenstein, S. J.; Raffy, C. *J. Phys. Chem. A* **2002**, *106*, 4904−4913.
(91) Miller, J. A.; Klippenstein, S. J. *Phys. Chem. Chem. Phys.* **2004**, *6*, 1192−1202.
(92) Miller, J. A.; Klippenstein, S. J. *J. Phys. Chem. A* **2004**, *108*, 8296−8306.
(93) Pitzer, K. S.; Gwinn, W. D. *J. Chem. Phys.* **1942**, *10*, 428−440.
(94) *NIST Standard Reference Database—Chemistry Webbook*; National Institute of Standards and Technology, 2003 (URL: http://webbook.nist.gov/chemistry/).
(95) Schmidt, V.; Zhu, G. Y.; Becker, K. H.; Fink, E. H. *Phys. Chem. Behav. Atmos. Pollut., Proc. Eur. Symp., 3rd* **1984**, 177.
(96) Hatakeyama, S.; Washida, N.; Akimoto, H. *J. Phys. Chem.* **1986**, *90*, 173−178.
(97) Van Look, H.; Peeters, J. *J. Phys. Chem.* **1995**, *99*, 16284−16289.
(98) Senosiain, J. P.; Miller, J. A.; Klippenstein, S. J. *Proc. Combust. Inst.* **2004**, *30*, 945−953.
(99) Miller, J. A.; Klippenstein, S. J. *J. Phys. Chem. A* **2001**, *105*, 7254−7266.